Wave energy absorption by a flap-type oscillating wave surge converter

By R. PORTER[1]† AND N. R. T. BIGGS[2]

[1]School of Mathematics, University of Bristol, Bristol, BS8 1TW, UK

[2]Department of Mathematics and Statistics, Whiteknights, PO Box 220, Reading RG6 6AX, UK

(Received ?; revised ?; accepted ?. - To be entered by editorial office)

This paper concerns the modelling of the wave energy absorbing qualities of a three-dimensional hinged flap-type wave energy converter closely related to the Oyster device‡. An analytic approach is taken to solving a set of boundary-value problems which arise from the decomposition of the linear water wave problem describing the interaction of the flap converter with waves into scattering and radiation potential problems. A novel integral equation formulation and numerical solution for approximating the solution of these boundary-value problems involving fixed and radiating thin barriers is also presented. Results concentrate on parameters likely to be close to those representing the Oyster device and attempt to expose features of Oyster that make it a successful wave energy absorber, despite theoretical results suggesting otherwise. Amongst the conclusions, it is shown that the length of flap is crucial in determining the optimal performance of the device.

1. Introduction

In this paper we develop an analytical approach for analysing a wave energy converter which models the Oyster device being developed by Aquamarine Power Ltd‡. A full scale prototype of the Oyster device has recently been deployed at the European Marine Energy Centre (EMEC) off the coast of Orkney in Scotland in late 2009. The mathematical model consists of a thin flat rectangular flap – or paddle – which is hinged along a horizontal axis above a sea bed in water of constant depth. The flap is buoyant and is thus orientated vertically upwards in calm water. Parallel-crested waves are incident on the flap and power is taken from the device from the rotation of the flap about the hinge. The Oyster device uses pistons attached at one end to the flap and at the other to a submersible base to drive a hydraulic system which generates power at an onshore generator, see (Whittaker & Folley 2012, figure 15).

Flap-type wave energy converters were largely overlooked in the early years of wave power development during the late 1970's and early 1980's. Inventors and engineers developing the first types of wave energy converters tended to be drawn towards more sophisticated devices often directed by the theoretical results being developed simultaneously by mathematicians. Thus, symmetrical devices such as flaps and paddles operating in surge/pitch were shown (independently by Mei (1976), Evans (1976) and Newman (1976)) to be at most 50% efficient in two-dimensions (that is, for a device spanning a

† Email address for correspondence: richard.porter@bris.ac.uk

‡ http://www.aquamarinepower.com/

narrow wave tank, where many of the ideas were first tested). When the fore-aft symmetry is broken greater efficiencies can be gained and such thinking led to the iteration of the Salter duck from an initial paddle design. Thus, efficiencies of close to 100% were reported for the Salter Duck, after Salter (1974), whose final design possessed a flat 'paddle' section at the front and a rounded section at the rear. Other examples in the class of 'terminator' device include the Bristol submerged cylinder (Evans *et al.* (1979)) which uses independent heave and surge modes of motion to again theoretically attain 100% efficiencies in two-dimensional wave tanks. Another cause for concern with flap-type converter centres on the issue of resonance. Most wave energy devices are naturally conceived and designed around the principle of resonance in which large resonant motions of the wave energy capturing device, when excited by incident waves, can be exploited to harness energy. Buoyant flap/paddle-type devices that are large enough to be used offshore beyond the surf zone typically have natural resonant periods which are too large compared to the range of periods found within sea spectra. This is true in the case of the Oyster which has a natural period reportedly around 20 seconds, see Whittaker & Folley (2012). Numerical modelling reported in Folley *et al.* (2007) and Whittaker & Folley (2012) suggests reducing the length of the flap or increasing its width can make the flap resonant within the range of periods of interest.

Despite these issues, the Oyster device has been successfully demonstrated in terms of numerical modelling, laboratory testing and now operationally at full scale. Thus, the 18m long prototype Oyster 1 unit rated at 315kW reportedly generates a mean power output of around 100kW: not exceptional given its size, but not insignificant and promising enough to attract further financial investment. The second-generation Oyster 800 project aims to install 3 separate units each with an installed capacity of 800kW and having a revised length of 26m. With theory suggesting that buoyant flap-type surge converters are not the most promising of solutions, it emerges as an intriguing prospect to investigate the analytical components and features of the model that allow this device to perform better than might be expected.

Despite the current interest in the Oyster device there are no sophisticated analytical models of the device and modelling is performed largely, it seems, using numerical panel-based hydrodynamic codes (see for example (Cruz 2008, §5)). However, recently Renzi & Dias (2012) have made some analytic progress considering infinite periodic arrays of flap-type devices as a means of determining interaction effects when a long array of flap-type devices are placed in a line. Yet it seems that an analytical approach to the problem of a single flap has not yet been tackled.

It is therefore the purpose of the present paper to carry out an analysis of a single flap-type converter. It is hoped that the results obtained from this analysis will be useful in verifying numerical methods and for quickly determining optimal parameters. One key parameter that emerges is the length of the flap as this sets, amongst other things, the so-called capture factor, being defined as the ratio of the length of incident wave crest absorbed by the device divided by the length of the device. If the flap is long compared to the wavelength, then it will react to the waves approximately as a two-dimensional device along most of its length and then the capture factor, according to the 50% maximum efficiency result in two-dimensions will be close to 0.5. If the device is short compared to the incident wavelength then it may react approximately as a point absorber (see Evans (1981) for example) and the capture factor may increase without bound; however, device motions must become increasingly large as the device becomes smaller to absorb the same amount of energy and eventually the theoretical basis for the model becomes redundant.

Analytically-based models of wave energy devices are often restricted to simple geome-

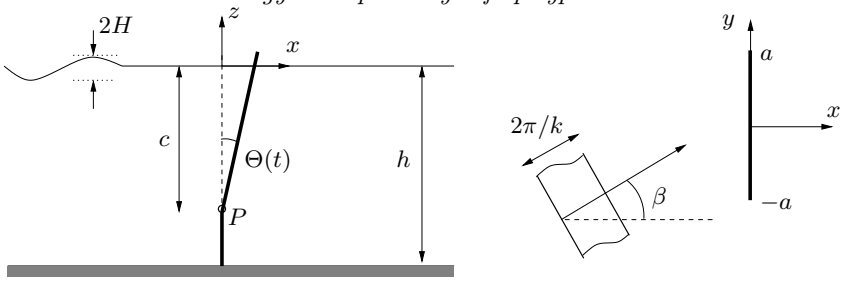

FIGURE 1. Some of the key parameters imposed on side and plan views of the flap converter configuration used in the hydrodynamic model.

tries and mainly in two-dimensional settings. In three-dimensions, calculations based on semi-analytical methods are often confined to single devices or arrays of devices consisting of absorbers with geometries having circular or spherical boundaries.

To investigate three-dimensional terminator-type devices of constant cross-section and finite length, one often has to resort to using numerically-based methods such as boundary-element panel-based codes. Approximations can be made to measure the effect of a finite length absorbers (see Evans (1980)). The flap-type device considered here is genuinely three dimensional, but the geometry of the flap being aligned in a plane of Cartesian coordinates allows analytic progress to be made, and we exploit the decomposition ideas recently presented by Renzi & Dias (2012) which were applied to a related problem of an infinite array of flap-type devices.

In §2 of the paper we derive expressions for the power absorption and relate them to certain properties of scattering and radiation potentials satisfying linear water wave problems. Much of this section is guided by principles of wave power conversion calculations set out, for example, in Thomas (2008). In §3, the boundary value problems are formulated for each of the two potentials and in §4, a new integral equation formulation and approximation to two-dimensional wave scattering and radiation problems involving thin barriers is derived and presented. §5 presents various useful relations that simplify the solution procedure including an outline of how embedding results are used to solve for all incident wave directions in terms of just one direction. In §6 we present results using parameters closely associated with the Oyster device and describe how the device works so well, giving some suggestions for further optimisation. Finally, we give conclusions and suggestions for future work in §7.

2. Formulation of the problem

Cartesian coordinates are defined with the origin in the mean free surface and z pointing vertical upwards. The bottom of the fluid of density ρ is on $z = -h$, a constant.

The hydrodynamic model assumes that the flap is thin and, at rest, that it occupies the vertical plane $\{x = 0, -a < y < a, -h < z < 0\}$. The flap is hinged along a horizontal axis $(x, z) = (0, -c)$ denoted in figure 1 by P, below which it remains fixed and above which it is free to move. We assume use of the standard small-amplitude theory of water waves.

The time-dependent problem is as follows. We define a velocity potential $\Phi(x, y, z, t)$ satisfiying

$$\nabla^2\Phi = 0, \qquad \text{in the fluid} \tag{2.1}$$

with linearised dynamic and kinematic free surface conditions

$$\Phi_t + g\zeta = 0, \quad \text{and} \quad \zeta_t = \Phi_z, \qquad \text{on } z = 0 \tag{2.2}$$

where $\zeta(x, y, t)$ denotes the free surface and g is gravitational acceleration. On the bottom of the fluid

$$\Phi_z = 0, \qquad \text{on } z = -h. \tag{2.3}$$

On the flap, the linearised kinematic condition is

$$\Phi_x(0^{\pm}, y, z, t) = \dot{\Theta}(t)u(z), \qquad \text{where} \qquad u(z) = \begin{cases} 0, & -h < z < -c \\ z + c, & -c < z < 0 \end{cases} \tag{2.4}$$

for $-a < y < a$ where $\Theta(t)$ is the (assumed small) angle measured anticlockwise from the vertical through which the flap has moved. Again, under the assumption of small angles, Newton's law applied to the rotational motion of the flap about the pivot, P, along $(x, z) = (0, -c)$ for $-a < y < a$ states that

$$I\ddot{\Theta}(t) = -C\Theta(t) + X_w(t) + X_e(t) \tag{2.5}$$

where I is the moment of inertia of the flap about the pivot P and C is the restoring torque/couple due to (presumed) buoyancy of the flap about P. These quantities can be calculated with some knowledge of the constitution of the flap (see §6). Thus C acts as a linear spring restoring force. Also in (2.5) X_w and X_e represent time dependent wave torques and external mechanical torques about P. These will be defined later.

Assuming an incident wave with time-harmonic dependence, all dependent variables respond with the same time dependence. Thus we write

$$\Phi(x, y, z, t) = \mathrm{Re}\{\phi(x, y, z)\mathrm{e}^{-\mathrm{i}\omega t}\}, \quad \zeta(x, y, t) = \mathrm{Re}\{\eta(x, y)\mathrm{e}^{-\mathrm{i}\omega t}\}, \quad \dot{\Theta}(t) = \mathrm{Re}\{\Omega\mathrm{e}^{-\mathrm{i}\omega t}\} \tag{2.6}$$

and

$$X_{w,e}(t) = \mathrm{Re}\{F_{w,e}\mathrm{e}^{-\mathrm{i}\omega t}\}. \tag{2.7}$$

We note that $\Theta(t) = \mathrm{Re}\{(\mathrm{i}\Omega/\omega)\mathrm{e}^{-\mathrm{i}\omega t}\}$ and the choice of using the complex angular velocity Ω as a proxy for the angular variation $\Theta(t)$ follows the typical approach to formulating wave energy problems. Now (2.5) is written

$$-\mathrm{i}\omega I\Omega = -\frac{\mathrm{i}C}{\omega}\Omega + F_w + F_e. \tag{2.8}$$

In the problem for ϕ we use linearity of the governing equations to decompose into two components, writing

$$\phi(x, y, x) = A\phi^S(x, y, z) + \Omega\phi^R(x, y, z) \tag{2.9}$$

where ϕ^S is responsible for scattering of incident waves of height H from a fixed flap and ϕ^R is responsible for wave radiation from the flap's own motion in the absence of an incident wave field. Here $A = -\mathrm{i}gH/(2\omega\psi_0(0))$ where ψ_0 will be defined a little below in (2.16).

Specifically, $\phi^{S,R}$ now satisfy the following:

$$\nabla^2\phi^{S,R} = 0, \qquad \text{in the fluid} \tag{2.10}$$

with a combined linear free surface condition

$$\phi^{S,R}_z - K\phi^{S,R} = 0, \qquad \text{on } z = 0 \tag{2.11}$$

where $K = \omega^2/g$ and

$$\phi^{S,R}_z = 0, \qquad \text{on } z = -h \tag{2.12}$$

with

$$\phi_x^S(0^\pm, y, z) = 0, \qquad \phi_x^R(0^\pm, y, z) = u(z), \qquad \text{for } -h < z < 0,\ |y| < a. \tag{2.13}$$

Since the radiation of waves by an oscillating flap generates a motion in $x > 0$ which is 180 degrees out of phase with the motion in $x < 0$ we must also impose an antisymmetry condition

$$\phi^R(0, y, z) = 0, \qquad \text{for } -h < z < 0,\ |y| > a \tag{2.14}$$

along with radiation conditions. For the scattering problem we first need to define the incident wave. Thus, for an incident wave of height H (amplitude $2H$) propagating at an anti-clockwise angle $\beta \in (-\pi/2, \pi/2)$ to the positive x-axis,

$$\phi^I(x, y, z) = \mathrm{e}^{\mathrm{i}k(x\cos\beta + y\sin\beta)}\psi_0(z) \tag{2.15}$$

where k is the positive wavenumber satisfying $K = k\tanh kh$, the usual dispersion relation, and

$$\psi_0(z) = N_0^{-1/2}\cosh k(z+h), \qquad N_0 = \frac{1}{2}\left(1 + \frac{\sinh 2kh}{2kh}\right) \tag{2.16}$$

is a normalised depth eigenfunction associated with propagating waves. We require both ϕ^R and $\phi^D \equiv \phi^S - \phi^I$ to represent outgoing waves at large distances from the flap.

The total couple on the pivot P due to wave forces is given by the integrated moment of the pressure forces acting in the positive x direction, or

$$X_w(t) = \rho\int_{-a}^{a}\int_{-h}^{0}\left[\Phi_t(0^+, y, z, t) - \Phi_t(0^-, y, z, t)\right]u(z)\,\mathrm{d}z\,\mathrm{d}y \tag{2.17}$$

using (2.4) which gives

$$F_w = -\mathrm{i}\omega\rho\int_{-a}^{a}\int_{-h}^{0}\left[\phi(0^+, y, z) - \phi(0^-, y, z)\right]u(z)\,\mathrm{d}z\,\mathrm{d}y. \tag{2.18}$$

We mimic the decomposition of ϕ by writing

$$F_w = AF_S(\beta) + \Omega F_R \tag{2.19}$$

where $F_S(\beta)$ is the exciting torque about P on a fixed flap due to an incident wave of normalised amplitude propagating at an angle β and F_R is the torque about P due to the forced motion of the flap itself. Thus we write

$$F_{S,R} = -\mathrm{i}\omega\rho\int_{-a}^{a}\int_{-h}^{0}\left[\phi^{S,R}(0^+, y, z) - \phi^{S,R}(0^-, y, z)\right]u(z)\,\mathrm{d}z\,\mathrm{d}y. \tag{2.20}$$

Moreover, it is typical to reduce the complex radiation torque into real and imaginary components which are in phase with angular velocities and accelerations respectively with

$$F_R = \mathrm{i}\omega\mathcal{A}(\omega) - \mathcal{B}(\omega) \tag{2.21}$$

where $\mathcal{A}(\omega)$ and $\mathcal{B}(\omega)$ are real coefficients called the added inertia and the radiation damping which vary with frequency and are computed by taking real and imaginary parts of (2.20), assuming the potential ϕ^R has been determined.

Then, according to (2.8) we have

$$-\mathrm{i}\omega I\Omega = -\frac{\mathrm{i}C}{\omega}\Omega + AF_S(\beta) + (\mathrm{i}\omega\mathcal{A} - \mathcal{B})\Omega + F_e. \tag{2.22}$$

In other words,

$$Z\Omega = AF_S + F_e, \qquad \text{with} \qquad Z = \mathcal{B}(\omega) - \mathrm{i}\omega(I + \mathcal{A}(\omega) - C/\omega^2). \tag{2.23}$$

We now specify the external force, envisaged to be a damping torque acting linearly against the angular velocity about the pivot P through which power is extracted by the flap. In other words we write

$$F_e = -\Lambda\Omega \tag{2.24}$$

where Λ is the power-take off parameter used to control the damping. Combining (2.24) with (2.23) gives

$$(Z + \Lambda)\Omega = AF_S(\beta). \tag{2.25}$$

Now the mean power is computed from the rate of working of the wave torque against the motion of the flap averaged over a period. In other words

$$W = \frac{1}{2\pi/\omega}\int_0^{2\pi/\omega} X_w(t)\dot{\Theta}(t)\mathrm{d}t \equiv \frac{1}{2}\mathrm{Re}\{F_w\Omega^*\} \tag{2.26}$$

(* denotes complex conjugation) in terms of time-independent quantities. From (2.8) we see that this gives

$$W = -\frac{1}{2}\mathrm{Re}\{F_e\Omega^*\} = \frac{1}{2}\Lambda|\Omega|^2 \tag{2.27}$$

after using (2.24) and assuming (fairly realistically) that Λ is real. Substituting in from (2.25) we have

$$W = \frac{1}{2}\frac{\Lambda|AF_S(\beta)|^2}{|Z+\Lambda|^2}. \tag{2.28}$$

Using the identity, for real Λ, that $2\Lambda(\mathrm{Re}\{Z\} + |Z|) = |\Lambda + Z|^2 - (\Lambda - |Z|)^2$ we find that

$$W = \frac{|AF_S(\beta)|^2}{4(\mathcal{B}+|Z|)}\left(1 - \frac{(\Lambda-|Z|)^2}{|\Lambda+Z|^2}\right). \tag{2.29}$$

For any given frequency W may take its optimal value of

$$W = W_{opt} = \frac{2\mathcal{B}}{\mathcal{B}+|Z|}\frac{|AF_S(\beta)|^2}{8\mathcal{B}} \tag{2.30}$$

provided $\Lambda = |Z|$. If, in addition, $\mathrm{Im}\{Z\} = 0$ and $\Lambda = \mathrm{Re}\{Z\}$, or

$$I + \mathcal{A}(\omega) = C/\omega^2 \qquad \text{and} \qquad \Lambda = \mathcal{B}(\omega) \tag{2.31}$$

then W takes a maximum value of

$$W = W_{max} = \frac{|AF_S(\beta)|^2}{8\mathcal{B}}. \tag{2.32}$$

The first of (2.31) is determined by hydrodynamics alone, and is satisfied when resonance is achieved; it states that inertia, including added inertia, is balanced by spring restoring forces. The second condition is tuneable. That is to say, if the first condition is satisfied at $\omega = \omega^*$, then setting the damping to $\Lambda = \mathcal{B}(\omega^*)$ ensures that the maximum power is extracted at $\omega = \omega^*$.

The power W, or indeed the maximum power W_{max}, is determined by the exciting force due to the incident wave. To determine a measure of the effectiveness of the device we need to normalise this. So, for example, the power per unit width of crest in an incident wave is given by

$$W_{inc} = \frac{1}{8}\rho g|H|^2 c_g, \qquad c_g = \frac{g}{2\omega}\left(\tanh kh + kh\,\mathrm{sech}\,kh\right) \tag{2.33}$$

and then the so-called 'capture width' of the wave energy converter is defined by

$$l = W/W_{inc} \qquad \text{having a maximum determined by} \qquad l_{max} = W_{max}/W_{inc}. \tag{2.34}$$

It is clear to see that by dividing the definition of W_{inc} into W and W_{max} that the dependence on the height of the wave vanishes, as it should. However, the dependence on β does not. The Haskind relation in three dimensions (e.g. Wehausen & Laitone (1960)) gives

$$W_{inc} = \frac{k}{16\pi\mathcal{B}} \int_0^{2\pi} |AF_S(\theta)|^2 \mathrm{d}\theta. \tag{2.35}$$

Thus it follows from (2.29) and (2.32) that

$$l = l_{max} \frac{2\mathcal{B}}{\mathcal{B} + |Z|} \left(1 - \frac{(\Lambda - |Z|)^2}{|\Lambda + Z|^2}\right) \tag{2.36}$$

where

$$l_{max} = \frac{2\pi |F_S(\beta)|^2}{k \int_0^{2\pi} |F_S(\theta)|^2 \, \mathrm{d}\theta} \tag{2.37}$$

is the maximum capture width attained when (2.31) are both satisfied. The optimal capture width is

$$l_{opt} = \frac{2\mathcal{B}}{\mathcal{B} + |Z|} l_{max} \tag{2.38}$$

which can be achieved when $\Lambda = |Z|$.

The capture width represents the equivalent crest-length of incident wave from which all the energy has been absorbed. It does not take into account the physical size of the absorbing device. Thus the 'capture factor' is defined as the capture width divided by the total length of the device. According to our problem this is,

$$\hat{l} = \frac{l}{2a}. \tag{2.39}$$

Economically, it makes sense to maximise this capture factor under certain constraints (for example, constraints on the amplitude of motion). This will be considered in the Results section.

In summary then, power and its other measures such as capture width and capture factor require the solution to two hydrodynamic problems, for $\phi^{S,R}$. In particular, it requires certain coefficients to be determined. These are $F_S(\theta)$ for all θ, the exciting forces on a fixed flap and $\mathcal{A}$ and $\mathcal{B}$, the added inertia and radiation damping for a radiation problem.

3. Specification of the scattering and radiation problems

3.1. *The scattering problem*

The problem for a fixed flap has been considered previously by many authors (e.g., Morse & Rubinstein (1938), Carr & Stelzriede (1952)). In this case we simply remove the depth dependence from the problem by writing

$$\phi^S(x, y, z) = \psi(x, y; \beta)\psi_0(z) \tag{3.1}$$

satisfying both (2.11), (2.12) whilst (2.10) reduces to

$$\left(\frac{\partial^2}{\partial x^2} + \frac{\partial^2}{\partial y^2} + k^2\right)\psi = 0, \tag{3.2}$$

in the plane of the free surface with (2.13) converted to

$$\frac{\partial\psi}{\partial x}(0^{\pm},y;\beta)=0,\qquad |y|<a, \tag{3.3}$$

and $\psi^D\equiv\psi-\psi^I$ represents diffracted outgoing waves at infinity where

$$\psi^I(x,y;\beta)=\mathrm{e}^{\mathrm{i}k(x\cos\beta+y\sin\beta)}. \tag{3.4}$$

The exciting wave torque about the pivot P is, from (2.20),

$$F_S(\beta)=-\mathrm{i}\omega\rho\int_{-a}^{a}\int_{-h}^{0}\left[\psi^D(0^+,y;\beta)-\psi^D(0^-,y;\beta)\right]\psi_0(z)u(z)\,\mathrm{d}z\,\mathrm{d}y \tag{3.5}$$

(since ψ^I is continuous). It helps now to decompose $u(z)$ in terms of the complete set of normalised depth eigenfunctions

$$\psi_n(z)=N_n^{-1/2}\cos k_n(z+h),\qquad N_n=\frac{1}{2}\left(1+\frac{\sin 2k_nh}{2k_nh}\right) \tag{3.6}$$

where k_n for $n=1,2,\ldots$ are the positive roots of $K=-k_n\tan k_nh$ and $\psi_n(z)$ including the definition for $n=0$ satisfy the orthogonality relation

$$\frac{1}{h}\int_{-h}^{0}\psi_n(z)\psi_m(z)dz=\delta_{mn}. \tag{3.7}$$

We can incorporate the definition of $\psi_0(z)$ into the above by writing $k_0=-\mathrm{i}k$. Then we write

$$u(z)=\sum_{n=0}^{\infty}U_n\psi_n(z) \tag{3.8}$$

which implies that

$$U_n=\frac{1}{h}\int_{-h}^{0}u(z)\psi_n(z)\,\mathrm{d}z=\frac{N_n^{-1/2}}{k_n^2h}\left[k_nc\sin k_nh+\cos k_nh-\cos k_n(h-c)\right] \tag{3.9}$$

after using the definition of $u(z)$ from (2.4). The integration in z in (3.5) evaluates to hU_0 from (3.7), and so (3.5) reduces to

$$F_S(\beta)=-\mathrm{i}\omega\rho U_0h\int_{-a}^{a}\left[\psi^D(0^+,y;\beta)-\psi^D(0^-,y;\beta)\right]\,\mathrm{d}y. \tag{3.10}$$

3.2. *The radiation problem*

For the wave radiation problem we exploit the fact that the condition (2.13) on the flap extends throughout the depth and depends only on z. That is, from (2.13) and (3.8)

$$\phi_x^R(0^{\pm},y,z)=\sum_{n=0}^{\infty}U_n\psi_n(z). \tag{3.11}$$

We can express the potential everywhere as a superposition of modes associated with the same set of depth modes, thus

$$\phi^R(x,y,z)=\sum_{n=0}^{\infty}U_n\phi_n(x,y)\psi_n(z) \tag{3.12}$$

in which (2.10) now implies

$$\left(\frac{\partial^2}{\partial x^2}+\frac{\partial^2}{\partial y^2}-k_n^2\right)\phi_n=0, \tag{3.13}$$

(when $n = 0$, $k_0 = -\mathrm{i}k$) in the plane of the free surface, with

$$\frac{\partial \phi_n}{\partial x}(0^{\pm}, y) = 1, \qquad -a < y < a \tag{3.14}$$

and $\phi_n(x, y)$ represents outgoing waves ($n = 0$) or decaying waves ($n \geqslant 1$) far from the origin. Also from (2.14)

$$\phi_n(0, y) = 0, \qquad |y| > a \tag{3.15}$$

whilst antisymmetry implies that $\phi_n(x, y)$ needs only be found in $x > 0$ with $\phi_n(-x, y) = -\phi_n(x, y)$ providing the extension to $x < 0$.

The property of this solution needed is again the wave torque about P defined by (2.20) and using (2.4), (3.8) and (3.12) this turns out to be given by

$$F_R = -2\mathrm{i}\omega\rho h \sum_{n=0}^{\infty} U_n^2 \int_{-a}^{a} \phi_n(0^+, y)\, \mathrm{d}y. \tag{3.16}$$

4. Solution of the scattering and radiation problems

4.1. *Scattering problem*

Solutions based on Green's functions are well documented (see for example, Linton & McIver (2001)). However, a much more direct solution is possible using Fourier transforms and the approach outlined below we believe to be new. First we note that (e.g. Linton & McIver (2001)) $\psi^D(x, y; \beta) = -\psi^D(-x, y; \beta)$ and so we only need the solution in $x > 0$ whilst the condition $\psi^D(0, y; \beta) = 0$ applies for $|y| > a$.

We define the Fourier transforms of $\psi^D(x, y)$ in $x > 0$, by

$$\bar{\psi}^D(x, l) = \int_{-\infty}^{\infty} \psi^D(x, y; \beta) \mathrm{e}^{-\mathrm{i}ly}\, \mathrm{d}y. \tag{4.1}$$

Then, taking Fourier transforms of the governing Helmholtz equation (3.2) gives

$$\left(\frac{d^2}{dx^2} + (k^2 - l^2)\right) \bar{\psi}^D(x, l) = 0. \tag{4.2}$$

The solution is given by

$$\bar{\psi}^D(x, l) = \bar{P}(l) \mathrm{e}^{-\lambda(l,k)x} \tag{4.3}$$

where

$$\lambda(l, k) = \sqrt{l^2 - k^2} = -\mathrm{i}\sqrt{k^2 - l^2}, \qquad \text{when } |l| < k \tag{4.4}$$

to ensure the correct outgoing wave behaviour at infinity. The integration constant is defined by letting $x \to 0$ so that

$$\bar{P}(l) = \int_{-\infty}^{\infty} \psi^D(0^+, y; \beta) \mathrm{e}^{-\mathrm{i}ly}\, \mathrm{d}y = \int_{-a}^{a} P(y; \beta) \mathrm{e}^{-\mathrm{i}ly}\, \mathrm{d}y \tag{4.5}$$

where we have used the abbreviation $P(y; \beta) = \psi^D(0^+, y; \beta)$ when $|y| < a$. Invoking the inverse transform we have, for $x > 0$,

$$\begin{aligned} \psi^D(x, y; \beta) &= \frac{1}{2\pi} \int_{-\infty}^{\infty} \bar{P}(l) \mathrm{e}^{-\lambda(l,k)x} \mathrm{e}^{\mathrm{i}ly}\, \mathrm{d}l \\ &= \frac{1}{2\pi} \int_{-\infty}^{\infty} \mathrm{e}^{-\lambda(l,k)x} \mathrm{e}^{\mathrm{i}ly} \int_{-a}^{a} P(y'; \beta) \mathrm{e}^{-\mathrm{i}ly'}\, \mathrm{d}y'\, \mathrm{d}l \end{aligned} \tag{4.6}$$

after using (4.5). If the order of integration is reversed, which can be done safely for $x > 0$, we find

$$\psi^D(x,y;\beta) = \int_{-a}^{a} P(y';\beta)\frac{1}{2\pi}\int_{-\infty}^{\infty} \mathrm{e}^{-\lambda(l,k)x}\mathrm{e}^{\mathrm{i}l(y-y')}\,\mathrm{d}l\,\mathrm{d}y' \tag{4.7}$$

which is the convolution result for inverse Fourier transforms. It is easy to confirm that this is equivalent to the Green's function approach described by Linton & McIver (2001) once the standard integral representation

$$H_0^{(1)}(k\rho) = \frac{1}{\pi\mathrm{i}}\int_{-\infty}^{\infty} \frac{\mathrm{e}^{-\lambda(l,k)|x-x'|}\mathrm{e}^{\mathrm{i}l(y-y')}}{\lambda(l,k)}\,\mathrm{d}l \tag{4.8}$$

with $\rho^2 = (x-x')^2 + (y-y')^2$ has been used for the Hankel function, being the key component of the Green's function for this problem. That is, (4.7) with (4.8) can be converted into the integral equation

$$\psi^D(x,y;\beta) = \frac{\mathrm{i}}{2}\int_{-a}^{a} P(y';\beta)\,\frac{\partial}{\partial x'}H_0^{(1)}(k\rho)\bigg|_{x'=0}\,\mathrm{d}y' \tag{4.9}$$

which coincides with Linton & McIver (2001, equation (4.142)). Pursuing the Green's function approach leads to some difficulties, as the account in Linton & McIver (2001) highlights. One possibility is to impose the boundary condition in such a way as to leave an integro-differential equation which can be integrated up; use can subsequently be made of Babinet's principle (see Linton & McIver (2001)) to relate solutions $P(y;\beta)$ to combinations of solutions to the complementary problem of a gap in an infinite breakwater where kernels in the integral operators are log-singular.

Another possibility is to impose the boundary condition on the flap in such a way as to leave a hypersingular integral equation for ψ^D on the flap, thus

$$-\frac{\partial\psi^I}{\partial x}(0,y;\beta) = \frac{\mathrm{i}}{2}\,\text{⨍}\!\!\!\!\!\!-_{-a}^{a} P(y';\beta)\,\frac{\partial^2}{\partial x\partial x'}H_0^{(1)}(k\rho)\bigg|_{x,x'=0}\,dy', \qquad |y|<a \tag{4.10}$$

where the integral is interpreted as a finite-part integral (see, for example, Linton & McIver (2001)). This approach requires some effort to manually integrate the singular parts of the kernel though this can be done with particular types of numerical approximation.

Instead we return to (4.6) and take derivatives in x throughout before letting $x \to 0^+$ for $|y| < a$ so that the boundary condition on the barrier (3.3) can be imposed. This gives

$$-\frac{\partial\psi^I}{\partial x}(0,y;\beta) = -\frac{1}{2\pi}\int_{-\infty}^{\infty}\lambda(l,k)\mathrm{e}^{\mathrm{i}ly}\int_{-a}^{a}P(y';\beta)\mathrm{e}^{-\mathrm{i}ly'}\,\mathrm{d}y'\,\mathrm{d}l, \qquad |y|<a. \tag{4.11}$$

It can be confirmed that the known behaviour of the unknown function $P(y';\beta) \sim (a^2-y'^2)^{1/2}$ leads to the inner integral behaving like $O(|l|^{-3/2})$ for large $|l|$, and this ensures convergence of the outer integral.

We now consider a numerical solution method to (4.11). Bearing in mind the end-point behaviour of $P(y;\beta)$ we write

$$P(y;\beta) \approx \sum_{p=0}^{2P+1}\alpha_p w_p(y/a), \qquad |y|<a, \qquad \text{where} \qquad w_p(t) = \frac{\mathrm{e}^{\mathrm{i}\pi p/2}}{(p+1)}\sqrt{1-t^2}\,U_p(t), \tag{4.12}$$

where $U_p(\cos\theta) = \sin(p+1)\theta/\sin\theta$ are Chebychev polynomials of the second kind and α_p

are coefficients to be determined. The numerical scaling factors anticipate later algebraic simplification.

Substituting (4.12) into (4.11), multiplying through by $(-1/\pi)w_q^*(y/a)$ and integrating over $|y| < a$ (for $q = 0, 1, \ldots, 2P+1$), a process characteristic of the Galerkin method, leads us to the following system of equations for the coefficients α_p:

$$\sum_{p=0}^{2P+1} \alpha_p K_{pq} = D_q(ka\sin\beta), \qquad q = 0, 1, \ldots, 2P+1 \tag{4.13}$$

where

$$\begin{aligned} K_{pq} &= \frac{1}{2\pi^2}\int_{-\infty}^{\infty} \lambda(l,k)\int_{-a}^{a} \mathrm{e}^{\mathrm{i}ly} w_q^*(y/a)\,\mathrm{d}y \int_{-a}^{a} \mathrm{e}^{-\mathrm{i}ly'} w_p(y'/a)\,\mathrm{d}y'\,\mathrm{d}l \\ &= \tfrac{1}{2}\int_{-\infty}^{\infty} \frac{D_p^*(\xi)D_q(\xi)}{\lambda^*(\xi,ka)}\,\mathrm{d}\xi, \end{aligned} \tag{4.14}$$

after a change of variables ($la = \xi$, $y/a = t$, $y'/a' = t'$), where we have defined

$$D_q(\xi) = -\lambda(\xi,ka)\frac{\mathrm{e}^{-\mathrm{i}\pi q/2}}{(q+1)\pi}\int_{-1}^{1} \mathrm{e}^{\mathrm{i}\xi t}(1-t^2)^{1/2}U_q(t)\,\mathrm{d}t. \tag{4.15}$$

Using Gradshteyn & Ryzhik (1981, §3.715 (13), (18)), for example, and properties of Bessel functions, J_q, we arrive at the results

$$D_q(\xi) = -\lambda(\xi,ka)J_{q+1}(\xi)/\xi, \quad \xi > 0, \qquad \text{and} \qquad D_q(0) = \tfrac{1}{2}\mathrm{i}ka\delta_{q0}. \tag{4.16}$$

It follows, using the relation $J_p(-\xi) = (-1)^p J_p(\xi)$, that $D_q(-\xi) = (-1)^q D_q(\xi)$ and so

$$K_{pq} = \tfrac{1}{2}\int_{-\infty}^{\infty} \frac{\lambda(\xi,ka)}{\xi^2}J_{p+1}(\xi)J_{q+1}(\xi)\,\mathrm{d}\xi = \tfrac{1}{2}(1+(-1)^{p+q})\int_0^{\infty} \frac{\lambda(\xi,ka)}{\xi^2}J_{p+1}(\xi)J_{q+1}(\xi)\,\mathrm{d}\xi \tag{4.17}$$

whilst

$$D_q(ka\sin\beta) = \mathrm{i}[\mathrm{sgn}(\beta)]^q \cot|\beta| J_{q+1}(ka\sin|\beta|), \quad \beta \neq 0 \tag{4.18}$$

with the case of $\beta = 0$ covered by (4.16). We note that, from (4.17), $K_{pq} = 0$ if $p+q$ is odd. This redundancy is typical of geometric configurations which possess lines of symmetry (as we have here along $y = 0$) which have not been exploited in the formulation. That is, we could have decomposed the scattering problem into components symmetric and antisymmetric about $y = 0$ from the outset.

An integral result involving products of Bessel functions (Gradshteyn & Ryzhik 1981, §6.538(2)) can be used to write

$$K_{2p+\nu,2q+\nu} = \frac{\delta_{pq}}{4q+2+2\nu} + \widetilde{K}_{2p+\nu,2q+\nu} \tag{4.19}$$

where

$$\widetilde{K}_{2p+\nu,2q+\nu} = \int_0^{\infty}\left(\frac{\lambda(\xi,ka)}{\xi^2} - \frac{1}{\xi}\right)J_{2p+1+\nu}(\xi)J_{2q+1+\nu}(\xi)\,\mathrm{d}\xi \tag{4.20}$$

for $\nu = 0, 1$, $p, q = 0, 1, \ldots$. Thus (4.13) is finally reduced to the decoupled pair of systems given by

$$\frac{\alpha_{2q}}{4q+2} + \sum_{p=0}^{P}\alpha_{2p}\widetilde{K}_{2p,2q} = D_{2q}(ka\sin\beta), \qquad q = 0, 1, \ldots, P \tag{4.21}$$

and

$$\frac{\alpha_{2q+1}}{4q+4} + \sum_{p=0}^{P} \alpha_{2p+1} \widetilde{K}_{2p+1,2q+1} = D_{2q+1}(ka\sin\beta), \qquad q = 0, 1, \ldots, P. \tag{4.22}$$

When $\beta = 0$, $D_q(0) = \frac{1}{2}\mathrm{i}ka\delta_{q0}$, and with the forcing now absent in (4.22), $\alpha_{2q+1} = 0$ for $q = 0, 1, \ldots$. This reflects the fact that normal incidence generates only a symmetric response and the antisymmetric component of the solution is absent.

The pair of systems (4.21), (4.22) have certain desirable properties including being symmetric and second-kind in structure. The integrals defining $\widetilde{K}_{pq}$ in (4.20) can be divided into separate parts from $0 < \xi < ka$ which are pure imaginary and from $ka < \xi < \infty$ which are real and in which the integrands decay like $O((ka)^2/\xi^4)$.

The final part of the solution requires us to calculate $F_S(\beta)$ given by (3.10). Substituting (4.12) into (3.10) after using the fact that ψ^D is an odd function gives

$$F_S(\beta) = -2\mathrm{i}\omega\rho U_0 ha \sum_{p=0}^{2P+1} \alpha_p \int_{-a}^{a} w_p(y/a)\,\mathrm{d}y = -\mathrm{i}\omega\rho U_0 ha\pi\alpha_0 \tag{4.23}$$

using (4.15), (4.16) so that the integral evaluates to $\frac{1}{2}\pi\delta_{p0}$.

We remark that the result (4.23) shows that, for the purposes of computing the exciting moment on the flap, only the symmetric system (4.21) for even coefficients is needed, although numerically one gets the system (4.22) for very little extra cost in the computational scheme.

4.2. *Radiation problem*

This problem can be solved in a manner identical to the scattering problem previously. Indeed, for $n = 0$, it is identical apart from the change to the boundary condition imposed on the flap and it is easy to confirm that

$$\phi_0(x, y) = \psi^D(x, y; 0)/(-\mathrm{i}k). \tag{4.24}$$

For $n \geqslant 1$ we follow the method used from the scattering problem to derive the integral equation for $\phi_n(0^+, y)$ on $|y| < a$ as

$$1 = \frac{\partial\phi_n}{\partial x}(0^+, y) = -\frac{1}{2\pi}\int_{-\infty}^{\infty} \gamma(l, k_n)\mathrm{e}^{\mathrm{i}ly} \int_{-a}^{a} \phi_n(0^+, y')\mathrm{e}^{-\mathrm{i}ly'}\,\mathrm{d}y'\,\mathrm{d}l, \qquad |y| < a, \tag{4.25}$$

the significant changes being the replacement of $\lambda(l, k)$ by $\gamma(l, k_n) \equiv \sqrt{l^2 + k_n^2}$ and the revised forcing term, whilst the potential in $x > 0$ is given by the integral representation

$$\phi_n(x, y) = \frac{1}{2\pi}\int_{-\infty}^{\infty} \mathrm{e}^{-\gamma(l,k_n)x}\mathrm{e}^{\mathrm{i}ly} \int_{-a}^{a} \phi_n(0^+, y')\mathrm{e}^{-\mathrm{i}ly'}\,\mathrm{d}y'\,\mathrm{d}l. \tag{4.26}$$

We again use the Galerkin method to approximate the solution of the integral equation by following (4.13) and writing

$$\phi_n(0^+, y) \approx a\sum_{p=0}^{P} \alpha_{2p}^{(n)} w_{2p}(y/a) \tag{4.27}$$

where $w_p(t)$ has been defined in (4.12) and $\alpha_{2p}^{(n)}$ are coefficients to be determined. Note that we have anticipated, through the inclusion of the set of even Chebychev polynomials only, that the uniform forcing on the flap in radiation will only generate solutions even in y.

Thus, following the approximation methods shown in the scattering problem, it is eventually found that we have a single even system given by

$$\frac{\alpha_{2q}^{(n)}}{4q+2} + \sum_{p=0}^{P} \alpha_{2p}^{(n)} \widetilde{K}_{2p,2q}^{(n)} = D_{2q}^{R}, \qquad q = 0, 1, \ldots, P \tag{4.28}$$

where, due to the boundary condition (3.14) on the flap, it turns out that

$$D_{2q}^{R} = -\frac{\delta_{q0}}{2} \tag{4.29}$$

and where $\widetilde{K}_{2p,2q}^{(0)} = \widetilde{K}_{2p,2q}$ is already given in (4.20) whilst for $n \geqslant 1$,

$$\widehat{K}_{2p,2q}^{(n)} = \int_0^\infty \left(\frac{\gamma(\xi, k_n a)}{\xi^2} - \frac{1}{\xi} \right) J_{2p+1}(\xi) J_{2q+1}(\xi)\, \mathrm{d}\xi \tag{4.30}$$

for $p, q = 0, 1, \ldots$. The noticable change in the above is the replacement of $\lambda(\xi, ka)$ by $\gamma(\xi, k_n a)$ which is as a result of the change of governing equation for ϕ_n when $n \geqslant 1$. Note that (4.30) is both real and symmetric for $n \geqslant 1$ and so $\alpha_{2p}^{(n)}$ are real for $n \geqslant 1$. On account of the relation (4.24) and the extra scaling factor of a in (4.27) we have immediately that $\alpha_{2p}^{(0)} = \alpha_{2p}/(-\mathrm{i}ka)$ in terms of the solution to (4.21) for $\beta = 0$.

For fixed n, the integrand in (4.30) decays like $O((k_n a)^2/\xi^4)$ but $k_n \sim n\pi/h$ so the integration range is increased for larger n and larger a/h. There may be some merit in subtracting off the leading order oscillatory behaviour of the Bessel functions explicitly although this is not explored here.

Finally, from (3.16) we have

$$F_R = -\mathrm{i}\omega\rho h a^2 \pi \sum_{n=0}^{\infty} U_n^2 \alpha_0^{(n)}. \tag{4.31}$$

5. Embedding and other relations

Embedding has been used to connect far-field diffracted wave amplitudes by expressing the solution for a wave incident from an angle β in terms of solutions for other independent wave angles β_1 and β_2. See Linton & McIver (2001) for a survey of the embedding literature.

Here it will be used to connect exciting moments for an arbitrary incident wave angle $\beta \in (-\frac{1}{2}\pi, \frac{1}{2}\pi)$ in terms of one incident angle β_1.

First, we return to (4.9) and used the large-argument asymptotics of the Hankel function to deduce, after some algebra, that

$$\psi^D(x, y; \beta) \sim \frac{\mathrm{i}}{2} \left(\frac{2}{\pi kr} \right)^{1/2} \mathrm{e}^{\mathrm{i}(kr - \pi/4)} D(\theta; \beta), \qquad \text{as } kr \to \infty \tag{5.1}$$

where $r = (x^2 + y^2)^{1/2}$ and $\tan\theta = y/x$ and where

$$D(\theta; \beta) = \mathrm{i}k \cos\theta \int_{-a}^{a} P(y'; \beta) \mathrm{e}^{-\mathrm{i}ky' \sin\theta}\, \mathrm{d}y' \tag{5.2}$$

plays the role of the diffraction coefficient, measuring the amplitude of circular waves travelling in the direction θ away from the fixed flap as a function of the incident wave angle, β, on which $P(y; \beta)$ depends. It is known that $D(\theta; \beta) = D(\beta; \theta)$ and modifying

previous work by Biggs (2006) we see that two embedding formulae are available:

$$(\sin\theta - \sin\beta)D(\theta;\beta) = \sum_{j=1}^{2} C_j(\sin\theta - \sin\beta_j)D(\theta;\beta_j) \tag{5.3}$$

and

$$P(y;\beta) = \sum_{j=1}^{2} C_j \left[P(y;\beta_j) - \mathrm{i}k(\sin\beta_j - \sin\beta)\int_{-a}^{y} P(y';\beta_j)\mathrm{e}^{-\mathrm{i}k(y'-y)\sin\beta}\,\mathrm{d}y'\right] \tag{5.4}$$

where

$$C_1 = \frac{(\sin\beta_2 - \sin\beta)D(\beta;\beta_2)}{(\sin\beta_2 - \sin\beta_1)D(\beta_1;\beta_2)}, \qquad C_2 = \frac{(\sin\beta_1 - \sin\beta)D(\beta;\beta_1)}{(\sin\beta_1 - \sin\beta_2)D(\beta_2;\beta_1)} \tag{5.5}$$

and β_1, β_2 are any two distinct angles in $(-\pi/2, \pi/2)$. The dependence on two solutions $P(y;\beta_1)$ and $P(y;\beta_2)$ can be reduced to dependence on just one by choosing $\beta_2 = -\beta_1 \neq 0$ and noting that the symmetry of the flap about $y = 0$ implies that $P(y;-\beta_1) = P(-y;\beta_1)$.

By comparing the exciting force, given by (3.10) with (5.2) we see that

$$F_S(\beta) = -2\mathrm{i}\omega\rho U_0 h D(0;\beta)/(\mathrm{i}k). \tag{5.6}$$

Assuming solutions for incident wave angles β_1 and β_2 have been determined and that, consequently, $F_S(\beta_1)$ and $F_S(\beta_2)$ are known then combining (5.3), (5.5) and (5.6) shows that

$$F_S(\beta) = \frac{\sin\beta_1(\sin\beta_2 - \sin\beta)D(\beta;\beta_2)F_S(\beta_1) - \sin\beta_2(\sin\beta_1 - \sin\beta)D(\beta;\beta_1)F_S(\beta_2)}{\sin\beta(\sin\beta_2 - \sin\beta_1)D(\beta_2;\beta_1)}. \tag{5.7}$$

In fact choosing $\beta_2 = -\beta_1 \neq 0$ and using symmetry to show that $F_S(-\beta_1) = F_S(\beta_2)$ whilst $D(\beta;-\beta_1) = D(-\beta;\beta_1)$ means that (5.7) can be expressed more simply in terms of one angle β_1 as

$$F_S(\beta) = \frac{F_S(\beta_1)}{2\sin\beta D(-\beta_1;\beta_1)}\left[(\sin\beta_1 + \sin\beta)D(-\beta;\beta_1) - (\sin\beta_1 - \sin\beta)D(\beta;\beta_1)\right] \tag{5.8}$$

for $\beta \neq 0$. Thus, in order to calculate $F_S(\beta)$ for any angle, β of incidence, we calculate the solution for a non-zero angle, β_1 of incidence and calculate $F_S(\beta_1)$ from (4.23), or from (5.6) where

$$D(\theta;\beta) = -\pi\sum_{p=0}^{2P+1}\alpha_p D_p^*(ka\sin\theta) = \mathrm{i}\pi\cot|\theta|\sum_{p=0}^{2P+1}\alpha_p[\mathrm{sgn}(\theta)]^q J_{p+1}(ka\sin|\theta|) \tag{5.9}$$

if $\theta \neq 0$ and $D(0;\beta) = \frac{1}{2}\mathrm{i}\pi ka\alpha_0$ which follows after use of (4.16).

Some care is needed computing $F_S(0)$ in (5.8) and taking limits as $\beta \to 0$ shows that

$$F_S(0) = \frac{F_S(\beta_1)}{D(-\beta_1;\beta_1)}\left[\tfrac{1}{2}\mathrm{i}\pi ka\alpha_0 - \tfrac{1}{8}\mathrm{i}\pi(ka)^2\sin\beta_1\alpha_1\right]. \tag{5.10}$$

Use can be made of the particular relation in this problem between F_S and the diffraction coefficient D in (5.6) combined with a result commonly referred to as the optical theorem (see (Mei 1983, pp.323–325)) expressed using the current definitions as

$$\int_0^{2\pi}|D(\theta;0)|^2\,\mathrm{d}\theta = -4\pi\mathrm{Im}\{D(0;0)\}. \tag{5.11}$$

Then, using $D(\beta;0) = D(0;\beta)$ and (5.6) in (5.11) we get

$$\int_0^{2\pi} |F_S(\theta)|^2 \,\mathrm{d}\theta = -4\pi \left(\frac{2\omega\rho U_0 h}{k}\right)^2 \mathrm{Im}\{D(0;0)\} = 4\pi \left(\frac{2\omega\rho U_0 h}{k}\right) \mathrm{Im}\{F_S(0)\}. \quad (5.12)$$

This relation is important as it simplifies the calculation of the denominator of (2.36), (2.37).

If $D_R(\theta)$ is the far-field radiated wave amplitude associated with the $n = 0$ component of the series defining ϕ^R in (3.12) defined by

$$\phi_0(x,y) \sim \frac{\mathrm{i}}{2}\left(\frac{2}{\pi kr}\right)^{1/2} D_R(\theta)\mathrm{e}^{\mathrm{i}(kr-\pi/4)}, \qquad \text{as } kr \to \infty \quad (5.13)$$

then it follows from (4.24), (5.1) that D_R is related to the diffraction coefficient in the scattering problem by

$$D_R(\theta) = \frac{D(\theta;0)}{-\mathrm{i}k}. \quad (5.14)$$

This means, from (5.6), that

$$F_S(\beta) = 2\mathrm{i}\omega\rho U_0 h D_R(\beta) \quad (5.15)$$

which is a (scaled) version of the Haskind relation (see Mei (1983), for example) noting that $D^R(\beta) = -D^R(\pi \pm \beta)$ are implied by symmetries in the radiation problem, a general result for arbitrary bodies connecting exciting forces to radiated wave amplitudes and established by using ϕ^R and ϕ^S in Green's second identity.

Note however that the connection in (5.14) seems rather more particular to this problem.

6. Results

The flap is of width $2b$, and length $2a$, extends from the pivot at $z = -c$ to the free surface and has a mean density of ρ_s. Then its mass $M_s = 4\rho_s bca$ and its moment of inertia in rotation about P is $I = \frac{1}{3}M_s(c^2 + b^2)$. The constant of proportionality in the buoyancy torque is given by $C = \frac{1}{2}M_w(1-s)gc$ where the mass of water displaced by the flap is given by $M_w = 4\rho bca$, where ρ is the fluid density, and $s = \rho_s/\rho = M_s/M_w$ is the specific gravity of the flap.

We define the following dimensionless quantities

$$\mu = \frac{\mathcal{A}}{\frac{1}{3}M_w c^2}, \quad \nu = \frac{\mathcal{B}}{\frac{1}{3}M_w c^2\omega}, \quad \hat{\Lambda} = \frac{\Lambda}{\frac{1}{3}M_w c^2\omega} \quad (6.1)$$

so that

$$\hat{Z} = \frac{Z}{\frac{1}{3}M_w c^2\omega} \equiv \nu - \mathrm{i}\left(s(1+(b/c)^2) + \mu - \tfrac{3}{2}(1-s)/Kc\right)$$

and

$$\hat{F}_S(\beta) = F_S(\beta)/(4\mathrm{i}\rho\omega U_0 h a) \quad (6.2)$$

which non-dimensionalises the torque on the flap by the torque on a section of length $2a$ of normally-incident waves on an infinitely-long flap. Under the definition (6.2) and according to (4.23), $\hat{F}_S(\beta) = -\frac{1}{4}\pi\alpha_0$ which is independent of all geometrical parameters associated with the flap and only depends on ka and β. In figure 2 we show the variation of $|\hat{F}_S(\beta)|$ with ka for $\beta = 0°$, $15°$, $30°$ and $60°$. These curves are generated either directly by setting β to each angle in turn or by using the embedding result given in

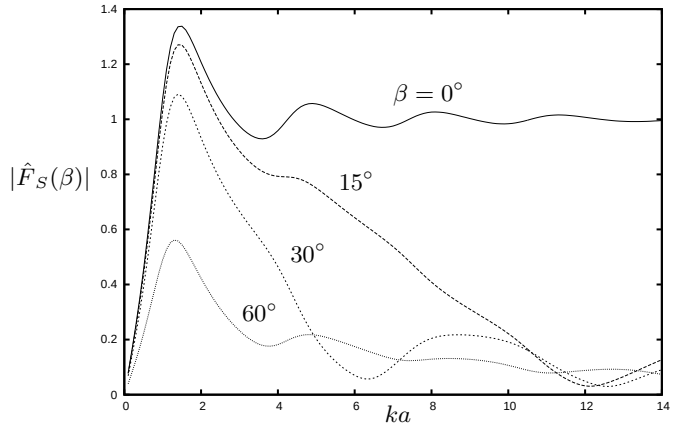

FIGURE 2. Modulus of the dimensionless exciting torque on a fixed plate against ka for different angles of incidence (shown against curves).

(5.8) with β_1 set to any non zero angle. We see from figure 2 that as $ka \to 0$, or the wavelength becomes large compared to the flap, the torque tends to zero, as expected. On the other hand, as ka increases and the wavelength becomes small compared to the flap, the torque due to normally incident waves ($\beta = 0$) tends to the torque for a section of equivalent length from an infinitely-long flap, again as expected. As $\beta \to 90°$, the force tends to zero, and there are signatures of interference from 'end effects' evident in the curves of $\beta = 15°$ and $\beta = 30°$. The result (5.12) has been confirmed numerically also by discretising the integral on the left-hand side and integrating numerically. The dimensionless version of (5.12) is $(2\pi/ka)\mathrm{Re}\{\hat{F}_S(0)\}$ and consequently, the dimensionless version of $\hat{l}_{max}$ is $|\hat{F}_S(\beta)|^2/(2\mathrm{Re}\{\hat{F}_S(0)\})$.

The numerical method relies on various numerical truncation parameters. The infinite integrals defining matrix entries in the numerical systems have been computed using 10-point Guass quadrature on a truncated integration range and with a discretisation scheme based on the 2π-oscillation period of Bessel functions. Numerical experimentation suggests that as few as $n = 5$ evanescent modes in the radiation problem and $P = 6$ modes in the Galerkin approximation are sufficient to achieve results which are accurate enough for graphical purposes in all cases presented. Accurate results are very quick to compute. Results have been computed independently using a collocation method applied to a hypersingular integral equation formulation to verify their accuracy.

We next consider the variation of added inertia μ and radiation damping ν with ka due to a flap in forced motion. As a means of verifying the results, we compare three-dimensional results defined by (6.1) with (2.21) and (4.31) with the equivalent flap in a two-dimensional setting. Thus, it is a simple matter to derive that the complex radiation torque on a section of length $2a$ from an infinitely-long flap, non-dimensionalised by the same factor used for the three-dimensional flap is

$$\hat{F}^R_{2D} = \frac{F^R_{2D}}{\frac{1}{3}M_w c^2\omega} = \mathrm{i}\mu_{2D} - \nu_{2D} = \frac{3\mathrm{i}h}{c^3 b}\sum_{n=0}^{\infty}\frac{U_n^2}{k_n} \tag{6.3}$$

where U_n is given by (3.9). The corresponding two-dimensional radiation potential, odd in x, is given, for $x > 0$, by

$$\phi^R_{2D}(x,z) = -\sum_{n=0}^{\infty}\frac{U_n}{k_n}\mathrm{e}^{-k_n x}\psi_n(z). \tag{6.4}$$

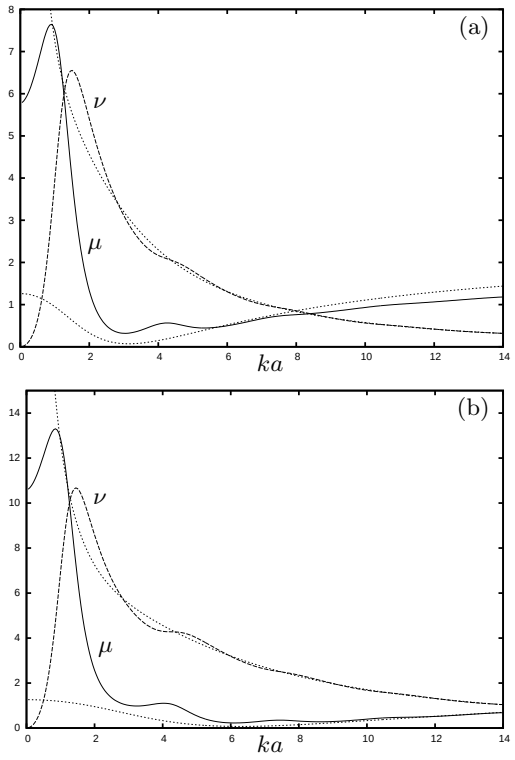

FIGURE 3. The variation of dimensionless added inertia μ (solid curve) and radiation damping ν (dashed curve) with ka and their two-dimensional counterparts (dotted curves): (a) $a/h = 1$; (b) $a/h = 2$.

We should expect that, for a long flap (a/h large) and for a high frequency (ka large) that the three-dimensional added inertia and damping tend to the equivalent two-dimensional results as the motion induced by the oscillating flap becomes more and more two-dimensional. This is clearly illustrated in figure 3(a), (b). Here we have chosen $s = 0.25$, $b/h = 0.1$, $c/h = 0.8$ and $a/h = 1$ in (a) and $a/h = 2$ in (b). The figures also illustrate typical behaviour namely, that radiation damping tends to zero in the low and high frequency limit and that the added inertia has non-zero limits at zero and infinity frequency.

Attention now turns to the energy absorping capacity of the flap-type converter whose hydrodynamic ingredients are the complex exciting torques and added inertia and damping coefficients previously discussed. Interest focuses on the capture factor, $\hat{l}$, defined by (2.39) and being the capture width of the device, l, defined by (2.36), divided by the length of the device, $2a$. Also of interest are maximum and optimal capture factors, $\hat{l}_{max}$ and $\hat{l}_{opt}$ defined by (2.37) and (2.38) divided by $2a$.

For a long device we expect $\hat{l}_{max}$ to tend to a half, as an infinitely-long device is two-dimensional with a maximum efficiency of a half owing to the fore-aft symmetry of the flap and its antisymmetric motion. For a short device $\hat{l}_{max}$ will increase towards infinity since $a \to 0$ but the capture width l tends to the point absorber result of $2/k$ for surge motion. So we expect to see $\hat{l}_{max} \to 1/ka$ as $ka \to 0$. This behaviour is seen clearly in figures 4(a)–(d) where $\hat{l}_{max}$ is plotted alongside dotted curves of $\hat{l} = 0.5$ and $\hat{l} = 1/(ka)$

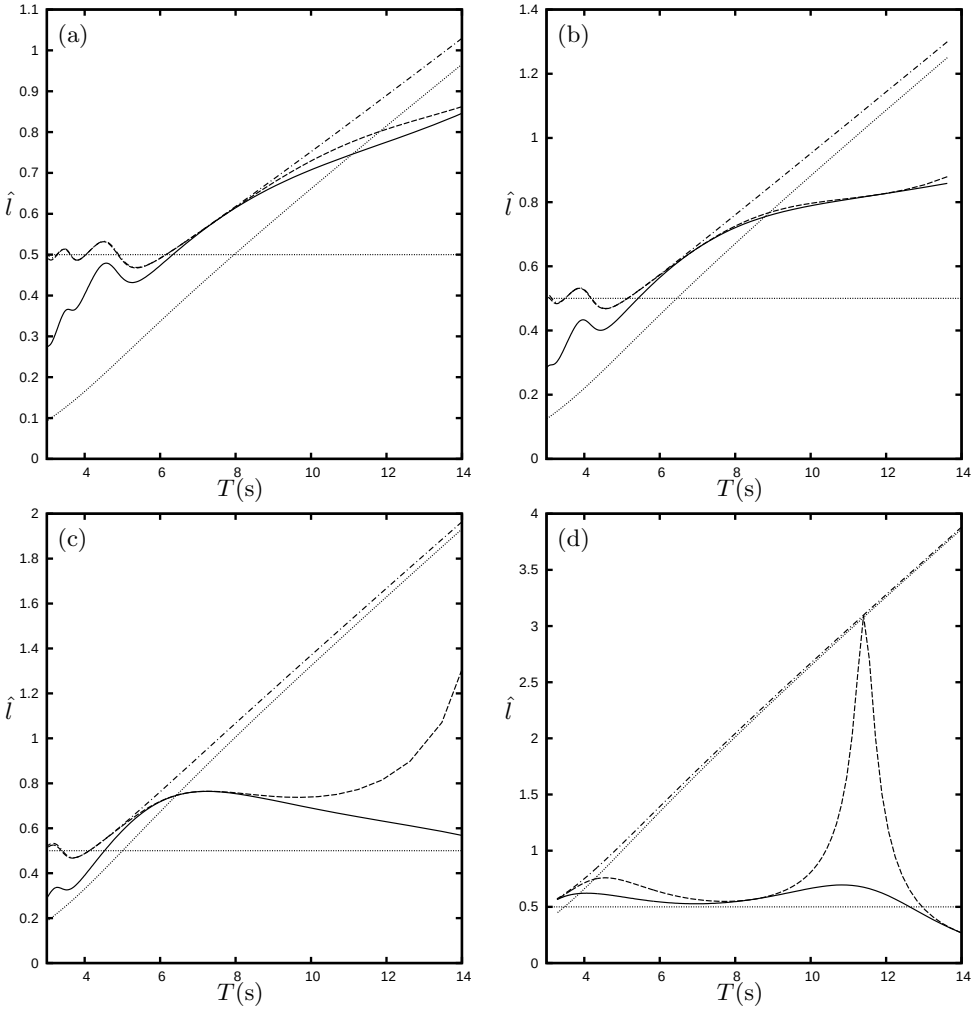

FIGURE 4. Capture factors as a function of wave period T in seconds for a flap of various lengths in water of depth 12m: (a) $a/h = 2$ ($2a = 48$m); (b) $a/h = 1.5$ ($2a = 36$m); (c) $a/h = 1$ ($2a = 24$m); (d) $a/h = 0.5$ ($2a = 12$m). In each case $b/h = 0.1$, $c/h = 0.8$ and $s = 0.25$, $\beta = 0$. The chained curve represents $\hat{l}_{max}$ and dotted curves are two-dimensional and point absorber asymptotes. The dashed curve is $\hat{l}_{opt}$ and the solid curves are particular simulations of $\hat{l}$ for fixed $\hat{\Lambda}$: (a)–(c) $\Lambda = 8$; (d) $\Lambda = 2$.

and variations in the length of the flap affect how rapidly one limit is approached over the same range of wave periods.

In figures 4(a)–(d) we have fixed certain parameters close to those that might represent the Oyster, so $s = 0.25$, $h = 12$m, $b/h = 0.1$ (so the width is $2b = 2.4$m) and $c/h = 0.8$ (hinged close to the sea-bed). For other parameters close to these the qualitative nature of the results shown in 4(a)–(d) remains largely the same. Thus, the variation throughout the sequence of four figures shows the effect of the length of the flap as it is varied from 48m in (a) to 12m in (d). Waves are normally-incident ($\beta = 0$) in all cases and it is assumed that the range of periods of interest lie between 5 and 12 seconds. It can be observed that $\hat{l}_{opt}$ can be very close to $\hat{l}_{max}$ over a broad range of periods (most notably small periods) even though it is never resonant over those periods. Resonance periods

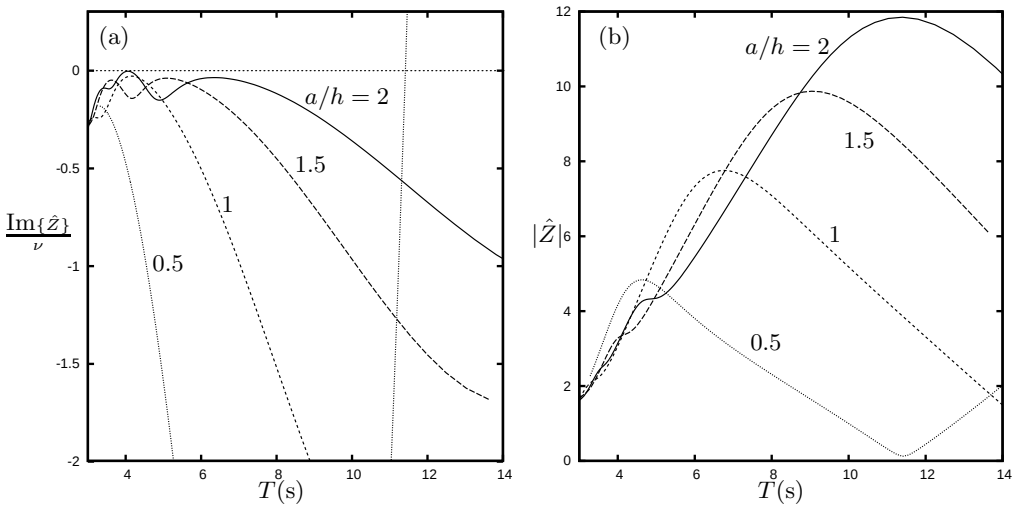

FIGURE 5. Variation of: (a) $\mathrm{Im}\{\hat{Z}\}/\nu$ and (b) $|\hat{Z}|$ with period T in seconds for the four cases in figure 4(a)–(d) (values of a/h shown against curves).

are indicated larger values of T where $\hat{l}_{opt} = \hat{l}_{max}$. As a/h is reduced the resonant period is also reduced and can eventually be identified as the tall narrow peak in $\hat{l}_{opt}$ in figure 4(d). These calculations seem to match those reported for the 18m long Oyster which has a 20s period and the numerical modelling of Whittaker & Folley (2012) which suggest capture factors over 0.7 and sea-spectrum averaged capture factors of around 0.5. For longer flaps than $a/h = 2.0$, the results are dominated by two-dimensional effects and capture factors are reduced to below 0.5 across the range of periods of interest. Likewise, for shorter flaps, the narrow resonant peak becomes dominant at the expense of high capture factors at periods outside the peak. Thus, a flap of intermediate length appears to enjoy a broad-banded capture factor which is mainly greater than 0.5. The results shown here suggest that the optimal length of flap might be close to 36m, but that figure could be dependent on other parameters assigned to the flap.

There are three ingredients in the determination of the capture factor. The first is decided by the geometry of the wave absorber being

$$\frac{|F_S(\beta)|^2}{\int_0^{2\pi} |F_S(\theta)|^2 \,\mathrm{d}\theta} \tag{6.5}$$

as this sets l_{max} and depends on scattering of waves by the fixed absorber. In order for this to be as high has possible, one needs a highly directional force profile as a function of wave angle. The flap offers this feature. The second factor is

$$\frac{2\mathcal{B}}{\mathcal{B} + |Z|} = \frac{2}{1 + (1 + (\mathrm{Im}\{Z\}/\mathcal{B})^2)^{1/2}} \tag{6.6}$$

which multiplies l_{max} to set l_{opt}. This is the most important feature and depends on hydrodynamic coefficients associated with radiation. The key to making l_{opt} as close to l_{max} is making the factor $\mathrm{Im}\{Z\}/\mathcal{B}$ as small as possible over a range of periods. Figure 3 illustrates two factors that makes this possible in the cases of $a/h = 1$ and $a/h = 2$, where the range of values of ka of interest are from $ka = 2$ up to $ka = 5$. Firstly, ν is much greater than μ and secondly, μ is decreasing with increasing ka (and hence increasing ω). The second observation allows the $\mathcal{A}(\omega)$ (along with the fixed I) to balance (not exactly, but at least approximately) the effect of the restoring force $-C/\omega^2$.

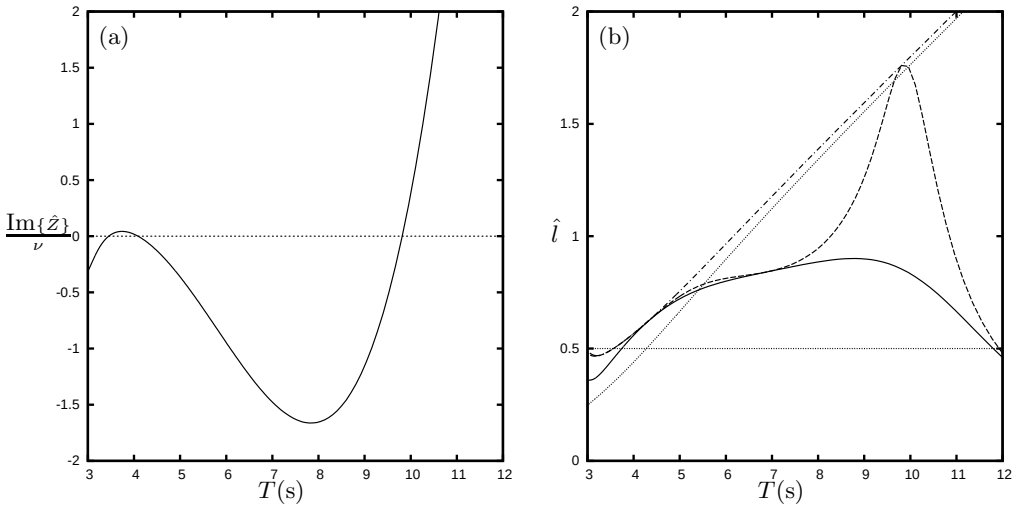

FIGURE 6. Variation of: (a) $\mathrm{Im}\{\hat{Z}\}/\nu$ and (b) capture factors $\hat{l}_{max}$, $\hat{l}_{opt}$ and $\hat{l}$ with period T in seconds for: $s = 0.2$, $h = 12$, $c/h = 0.8$, $a/h = 0.75$, $b/h = 0.2$, $\hat{\Lambda} = 2.25$.

These observations are shown graphically in figure 5(a) where the dimensionless quantity $\mathrm{Im}\{\hat{Z}\}/\nu \equiv \mathrm{Im}\{Z\}/\mathcal{B}$ is plotted against period for each of the four flap lengths in figure 4(a)–(d). To allow the vertical scale to be put into perspective, when $|\mathrm{Im}\{\hat{Z}\}/\nu| > 2\sqrt{2}$, $l_{opt} < \frac{1}{2} l_{max}$ and $|\mathrm{Im}\{\hat{Z}\}/\nu| < 1$ means that l_{opt} is more than 80% of l_{max}.

The final factor to play a part is

$$1 - \frac{(\Lambda - |Z|)^2}{|\Lambda + Z|^2} \tag{6.7}$$

the only point at which the controllable power take off is introduced. Here, we are looking for Λ to be close to $|Z|$ over a broad range of periods. Thus in figure 5(b) we plot $|\hat{Z}|$ for the four cases in figure 4(a)–(d). There is substantial variation in all cases. However, in the case of $a/h = 1.5$ corresponding to a flap length of 36m, there is a turning point in $|\hat{Z}|$ in the middle of the range of periods of interest, favouring the maximisation of (6.7) over that range of periods.

Optimisation of the performance of the device involves finely tuning these three components so that each is optimised in unison. But the explanation given above suggests mathematical reasons as to why the flap-type wave energy converter works so well.

Figure 5(a) also indicates that there may be the possibility of generating multiple resonances (periods when $\mathrm{Im}\{Z\} = 0$) spanning the range of periods of interest and this might be a route to optimising the power output of the flap. Without having performed a sophisticated optimisation process, we present a case arrived at by hand which illustrates such features. Thus we have chosen some parameters which might stretch the validity of the model. They are: $s = 0.2$, $c = 0.8$, $h = 12$m, $b/h = 0.2$ and $a/h = 0.75$; the flap is twice the width and more buoyant than in previous examples. Figure 6(a) presents the variation of $\mathrm{Im}\{\hat{Z}\}/\nu$ with period and shows there are 3 resonant periods, the crucial difference being the rebalancing of the rotational inertia effects against hydrodynamic effects. The corresponding capture factors (maximum, optimal and a simulation for $\hat{\Lambda} = 2.25$) are given in 6(b) illustrating that broad-banded capture factors over periods 5-10 seconds averaging roughly 0.8 are attainable. Whittaker & Folley (2012, figure 10), have also suggested multiple resonances are possible and they considered a 50m flap, increasing

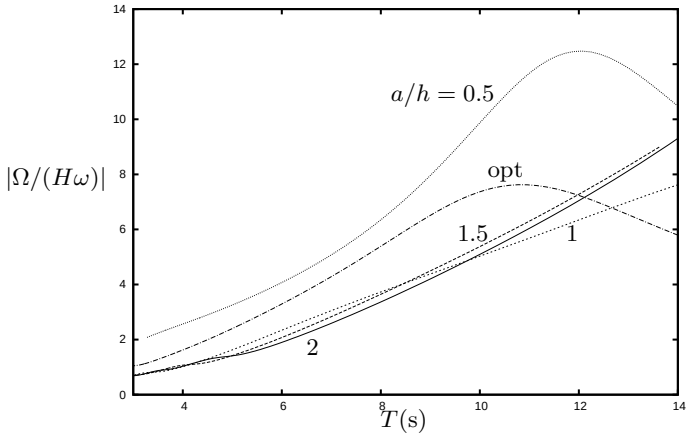

FIGURE 7. Angles (in degrees) of excursion of the flap per metre height of incident wave against period for the four cases in figure 4(a)–(d) and the 'optimised' flap in figure 6.

the flap-width to 5m. We have not been able to reproduce multiple resonances for such a configuration using our thin-barrier hydrodynamic model.

The final part of the results needs to address the question of flap excursion. From (2.25) we are able to calculate the maximum angle of rotation of the flap per unit height of incident wave, equivalent to

$$\left|\frac{\Omega}{H\omega}\right| = \frac{1}{h}\frac{3h^3}{8Kc^3b}\frac{|\hat{F}_S(\beta)|}{|\hat{Z}+\hat{\Lambda}|} \tag{6.8}$$

This is a dimensional quantity. For linear theory to retain validity, this quantity should be as small as possible although it is probably acceptable for angles below 15°. Figure 7 shows the variation of this quantity for the four cases in figure 4(a)–(d) and the 'optimised' flap of figure 5, and in each case $|\Omega/H\omega| < 13°$.

A smaller device needs to move further to exploit this energy capture, and hence there is a play-off between the potential for a higher capture factor and amplitudes of motion/acheivable power absorption.

We have not shown results for power absorption from angles of wave incidence other than normal incidence here; there is a reduction, as expected, in capture factor with increasing wave obliqueness. A measured sea spectrum which includes a wave spreading function could be used to determine actual power take off in a particular marine environment and help optimise flap parameters.

7. Conclusions

In this paper, an analytical approach to calculations assessing the efficacy of a three-dimensional flap-type wave energy converter model of the Oyster device have been made. The conclusions of the results presented appear to align with those used by Whittaker & Folley (2012) in the design process of the Oyster device. In particular, results suggest that there is an optimal length of flap which is somewhere around 30m and close to the 26m being proposed as part of the second-generation 'Oyster 800' project. A rough estimate of the results produced here would suggest a mean capture factor of about 0.65 for a 26m device and if the total incident wave energy were estimated at about 24kW/m then the mean power output would equate to approximately 400kW. Once compensation

is made for non-linear effects and losses in power take off mechanisms, this would again appear to be in line with recorded power outputs from Oyster.

Despite a lack of resonance within the range of energy-dense periods in the sea spectrum, the device exhibits near-resonance and hence broad-banded power absorption characteristics especially at low to intermediate wave periods. This feature is attributed to the large ratio between radiation damping and added inertia and it is supposed that this is presumably because of the high wave making capacity of a long oscillating flap which protrudes through the water surface. Suggestions, similar to those presented by Whittaker & Folley (2012) for making the flap multi-resonant leading to a larger capture factor of around 0.8 have been made.

The analytical treatment of this three-dimensional wave energy problem has produced a novel semi-analytical approach to solving problems involving finite barriers excited by incident waves or in motion. The numerical solution is simple to implement and fast and accurate. A simple adaptation of this method could be applied to the classic problem of wave scattering by an infinite thin breakwater with one, or a finite number, of gaps; see Linton & McIver (2001), Biggs *et al.*Biggs *et al.* (2000).

The solution method, based on Fourier transforms, allows an extension to be considered which considers the effects of a finite number of flaps in arbitrary parallel arrangements. Here, the interest would lie in how to optimise the so-called q-factor which measures the benefits of mutual wave interaction over isolated devices. More complicated extensions could include adding non-zero thickness to the flap in the hydrodynamic model. Two flaps placed back-to-back could improve wave energy absorption, as Srokosz & Evans (1979) illustrated in two-dimensions where maximum efficiencies were raised from 50% to 100%.

REFERENCES

Biggs, N. R. T., Porter, D. & Stirling, D. S. G. 2000 Wave diffraction through a perforated breakwater. *Q. J. Mech. appl Math.* **53**(3), 375–391.

Biggs, N. R. T. 2006 A new family of embedding formulae for diffraction by wedges and polygons. *Wave Motion* **43**(7), 517–528.

Carr, J. H. & Stelzriede, M. E. 1952 Diffraction of water waves by breakwaters. *US Nat. Bur. Stds.* **521**, 109–125.

Cruz, J. 2008 Numerical and experimental modelling of WECs In *Ocean Wave Energy.* (ed. J. Cruz) Springer, pp.133–188.

Evans, D. V. 1976 A theory for wave-power absorption by oscillating bodies. *J. Fluid Mech.* **77**, 1–25.

Evans, D. V. 1980 Some analytical results for two- and three-dimensional wave-energy absorbers. In *Power from Sea Waves* (ed. B. Count), pp.213–249.

Evans, D. V. 1981 Power from water waves. *Ann. Rev. Fluid Mech.* **11** 157–187.

Evans, D. V., Jeffrey, D. C., Salter, S. H. & Taylor, J. R. M. 1979 Submerged cylinder wave-energy device: theory and experiment. *Appl. Ocean Res.* **1**, 3–12.

Folley, M., Whittaker, T. W. T, & van't Hoff, J. 2007 The design of small seabed-mounted bottom-hinged wave energy converters. In *Proc. 7th European Wave and Tidal Conf. Porto, Portugal.*

Gradshteyn, I. S. & Ryzhik, I. M. 1981 *Tables of Integrals, Series and Products* New York: Academic Press.

Linton, C. M. & McIver, P. 2001 *Handbook of Mathematical Techniques for Wave/Structure Interactions* Chapman & Hall CRC.

Mei, C. C. 1976 Power extraction from water waves. *J. Ship Res.* **20**, 63–66.

Mei, C. C. 1983 *The Applied Dynamics of Ocean Surface Waves* Wiley Interscience, New York.

Morse, P. M. & Rubinstein, P. J. 1938 The diffraction of waves by ribbons and slits. *Phys. Rev.* **54**, 895–898.

Newman, J. N. 1976 The interaction of stationary vessels with regular waves. *Proc. Symp. Naval Hydrodyn. 11th, London* pp.491–501.

Renzi, E. & Dias, F. 2012 Resonant behaviour of an oscillating wave energy converter in a channel. *J. Fluid Mech.* **701**, 482–510.

Salter, S. H. 1974 Wave power *Nature* **249**, 720–724.

Srokosz, M. A. & Evans, D. V. 1979 A theory for wave-power absorption by two independently oscillating bodies *J. Fluid Mech.* **90**, 337–362.

Thomas, G. P. 2008 The theory behind conversion of ocean wave energy: a review. In *Ocean Wave Energy*. (ed. J. Cruz) Springer, pp.41–91.

Wehausen, J. V. & Laitone, E. V. 1960 Surface Waves. *Handbuch der Physik* **9**, 446–778.

Whittaker, T. W. T & Folley, M. 2012 Nearshore oscillating wave surge converters and the development of Oyster. *Phil. Trans. Roy. Soc. Lond. A.* **370**, 345–364.